

Baryonic fraction in the cold plus hot dark matter universe

Eunwoo Choi^{1†} and Dongsu Ryu^{2,3†}

¹*Department of Astronomy & Atmospheric Sciences, Kyungpook National University, Taegu 702-701, Korea*

²*Department of Astronomy & Space Science, Chungnam National University, Daejeon 305-764, Korea*

³*Department of Astronomy, University of Washington, Box 351580, Seattle, WA 98185*

Accepted 1997 ** **. Received 1997 ** **; in original form 1997 ** **

ABSTRACT

We report a study to constrain the fraction of baryonic matter in the cold plus hot dark matter (CHDM) universe by numerical simulations which include the hydrodynamics of baryonic matter as well as the particle dynamics of dark matter. Spatially flat, *COBE*-normalized CHDM models with the fraction of hot component $\Omega_h \leq 0.2$ are considered. We show that the models with $h/n/\Omega_h = 0.5/0.9/0.1$ and $0.5/0.9/0.2$ give a linear power spectrum which agrees well with observations. Here, h is the Hubble constant in unit of 100 km/s/Mpc and n is the spectral index of the initial power spectrum. Then, for the models with $h/n/\Omega_h = 0.5/0.9/0.2$ and baryonic fraction $\Omega_b = 0.05$ and 0.1 we calculate the properties of X-ray clusters, such as luminosity function, temperature distribution function, luminosity-temperature relation, histogram of gas to total mass ratio, and change of average temperature with redshift z . Comparison with the observed data of X-ray clusters indicates that the model with $\Omega_b = 0.05$ is preferred. The *COBE*-normalized CHDM model with $\Omega_b > 0.1$ may be ruled out by the present work, since it produces too many X-ray bright clusters.

Key words: galaxies: clusters of – hydrodynamics – cosmology: large-scale structure of Universe – x-ray: general.

1 INTRODUCTION

The large-scale structure of the universe forms when matter accretes onto high density perturbations via gravitational instability. Among the models that attempt to explain the quantitative features of the large-scale structure, the cold dark matter (CDM) model is based on the assumption that the dominant component of matter is cold. The model also assumes that the initial fluctuations are adiabatic and random Gaussian, and have a Zel'dovich spectrum, $P(k) = Ak^n$ with $n \sim 1$. The standard CDM (SCDM) model, which is the simplest and yet the most widely studied, makes the additional assumptions that the total $\Omega = 1$ and $\Omega_b \sim 0.05$ from the standard big bang nucleosynthesis (Walker et al. 1991). Here Ω is the density parameter. This model had some success, but it is now well known to have difficulties in explaining a number of observations (see, e.g., Ostriker & Steinhardt 1995). In particular, this model has excessive power on small scales when normalized to the *COBE* data on large scales (see, e.g., Bunn, Scott & White 1995). Several alterna-

tive cosmological models, including the CHDM model, have been studied claiming better agreement with observations.

The CHDM model is based on the same assumptions as the SCDM model, except that in addition to the CDM component, it has also the hot dark matter (HDM) component. HDM is composed of one of the three known species of neutrinos (ν_τ, ν_μ, ν_e) with a mass of $91.5\Omega_h h^2$ eV. Since neutrino's free streaming erases fluctuations in density on scales from galaxies to clusters during the radiation-dominated era, replacing a portion of CDM with HDM suppresses power on small scales. Therefore, the CHDM model has less power on small scales than the SCDM model. This basic property of the CHDM model was investigated some time ago (Fang, Li & Xiang 1984; Valdarnini & Bonometto 1985; Achilli, Occhionero & Scaramella 1985).

The fact that the CHDM model is promising in explaining the observed data of large-scale structure was first established by several analytic calculations using linear or nonlinear tools (Schaefer, Shafi & Stecker 1989; Van Dalen & Schaefer 1992; Holtzman & Primack 1993; Pogosyan & Starobinsky 1995; Dodelson, Gates & Stebbins 1996; Ma 1996; Borgani et al. 1995, 1997). For example, Holtzman & Primack (1993) used the peaks formalism for Gaussian density fields and found that the correlation function of clusters

† E-mail: ewchoi@vega.kyungpook.ac.kr;
ryu@sirius.chungnam.ac

in the CHDM model with $\Omega_h = 0.3$ is consistent with the correlation function of the Abell clusters.

A number of numerical simulations further confirmed the promising aspects of the CHDM model (Davis, Summers & Schlegel 1992; Klypin et al. 1993; Jing et al. 1994; Klypin & Rhee 1994; Nolthenius, Klypin & Primack 1994; Jing & Fang 1994; Yepes et al. 1994; Bryan et al. 1994b; Ghigna et al. 1994; Bonometto et al. 1995; Walter & Klypin 1996; Klypin, Nolthenius & Primack 1997; Davé et al. 1997). Most of these simulations were carried out for the model with the “standard” density ratio $\Omega_c/\Omega_h/\Omega_b = 0.6/0.3/0.1$. For example, Klypin & Rhee (1994) calculated the correlation function for the Abell clusters and the APM clusters and confirmed the results given by Holtzman & Primack (1993). Jing & Fang (1994) calculated the evolution of the mass function, the velocity dispersion function, and the temperature function of clusters and argued that their results favor the CHDM model over others. Bryan et al. (1994b) computed the properties of X-ray clusters using a code which can handle the hydrodynamics of baryonic matter. They showed that the luminosity and temperature distribution functions fit well the available observational data, and $\Omega_b \lesssim 0.1$ is sufficient to explain the X-ray properties in the CHDM model with $\Omega_h = 0.3$. Klypin et al. (1997) showed that the CHDM model with the “standard” density ratio, as well as that with $\Omega_h = 0.2$, give good fits to a wide variety of “present-epoch” data.

However, the CHDM model with $\Omega_c/\Omega_h/\Omega_b = 0.6/0.3/0.1$ has a problem in producing galactic halos at $z \gtrsim 3$ massive enough to account for neutral gas observed in damped Ly α systems (Mo & Miralda-Escudé 1994; Kauffmann & Charlot 1994; Ma & Bertschinger 1994; Klypin et al. 1995; Bi, Ge & Fang 1995). So it was suggested that the more promising version of the CHDM model should have less mass in the hot component, $\Omega_h \lesssim 0.2$, in order to have more power on galaxy scales and so produce significantly more high-redshift objects. Ma (1996), using an approximation to the evolution of linear power spectrum, argued that the slightly tilted ($n \sim 0.9 - 0.95$) CHDM model with $\Omega_h \sim 0.1 - 0.2$ gives a power spectrum that agrees best with the observed power spectrum. Primack et al. (1995) showed that dividing the neutrino mass between two species of neutrinos (ν_τ, ν_μ) lowers the power spectrum on the cluster scale, and thus lowers the cluster abundance without the necessity of tilt $n < 1$ of the CHDM model.

In this paper, we constrain Ω_b in the CHDM models with $\Omega_h \leq 0.2$ by investigating the properties of X-ray clusters that are sensitive to Ω_b . Recent satellite X-ray observations made the properties of X-ray clusters increasingly important to cosmology as a probe into the large-scale structure of the universe. Being massive and rare, the cluster abundance in the local and distant universe carries vital information on the initial density fluctuations and the matter content of the universe. Also being relatively young dynamically, the details of their structures provide us with some signatures left over from the formation epoch as well as information on the background cosmology. The study on the properties of X-ray clusters in model universe has been made analytically (e.g., Kitayama & Suto 1996) or numerically using grid-based codes (Kang et al. 1994; Cen & Ostriker 1994; Bryan et al. 1994a; Bryan et al. 1994b) and the SPH code (e.g., Evrard, Metzler & Navarro 1996). A general consen-

Table 1. Model Parameters.

Parameter	CHDMa	CHDMb	CHDMc	CHDMd
h	0.5	0.5	0.5	0.5
n	0.9	0.9	0.9	0.9
Ω_c	0.75	0.7	0.85	0.8
Ω_h	0.2	0.2	0.1	0.1
Ω_b	0.05	0.1	0.05	0.1
σ_8	0.67688	0.67688	0.73921	0.73921

sus seems to be that the SCDM model with $h = 0.5$ normalized to the *COBE* measurement of the anisotropies in the cosmic background radiation (i.e., $\sigma_8 > 1$) has serious difficulties in explaining the observed properties of X-ray clusters, such as the cluster abundance (Kang et al. 1994; Bryan et al. 1994a), the baryon fraction in clusters (Lubin et al. 1995), and the contribution of cluster emission to the X-ray background (Kang et al. 1994; Bryan et al. 1994a; Kitayama & Suto 1996). On the other hand, a flat CDM model with cosmological constant (Λ CDM) and a CHDM model, both of which have smaller values of σ_8 , seem more consistent with observations (Cen & Ostriker 1994; Bryan et al. 1994b). Here, σ_8 is the present-epoch, linear rms mass fluctuation in the sphere of radius $8h^{-1}$ Mpc.

We should mention that our work bears many similarities with that of Bryan et al. (1994b). Both consider X-ray clusters in the CHDM universe with similar (but not same) codes. However, while Bryan et al. (1994b) considered the CHDM model with $\Omega_c/\Omega_h/\Omega_b = 0.6/0.3/0.1$, which was “standard” at that time, we considered the models with a smaller Ω_h ($\Omega_h = 0.2$, see §3.2), which are more acceptable now.

In §2 the details of the numerical simulations are described. Results are presented in §3. Conclusion follows in §4.

2 NUMERICAL SIMULATIONS

2.1 Choice of Models

In order to study the linear power spectrum using analytic approximations in the CHDM universe, Ma (1996) considered the models with $0.5 \leq h \leq 0.8$, $0.8 \leq n \leq 1$, and $0.05 \leq \Omega_h \leq 0.3$. The normalization of the power spectrum, σ_8 , was determined by the *COBE* observation (see §2.2 for details). As mentioned in Introduction, Ma (1996) found that the models with $n \sim 0.9 - 0.95$ and $\Omega_h \sim 0.1 - 0.2$ give power spectra that agree well with observation. Here, we adopt Ma’s models with $h/n/\Omega_h = 0.5/0.9/0.1$ and $0.5/0.9/0.2$. For baryonic fraction we use the values $\Omega_b = 0.05$ and 0.1 , which is in the range predicted by big bang nucleosynthesis $0.007h^{-2} \lesssim \Omega_b \lesssim 0.024h^{-2}$ (Walker et al. 1991; Copi, Schramm & Turner 1995). The values of the model parameters are summarized in Table 1.

2.2 Initial Power Spectrum

Assuming the density distribution is Gaussian random, the initial condition is determined by the power spectrum only. It is given by the following functional form

$$P(k, a, \Omega_h) = a^2 A k^n T^2(k, a, \Omega_h), \quad (1)$$

where $a = (1+z)^{-1}$ is the expansion parameter, A is a normalization constant, and k is the wave number. $T(k, a, \Omega_h)$ is the transfer function describing linear changes in the perturbation. We adopt the transfer function derived by Ma (1996). For CDM, it is given by

$$T_c(k, a, \Omega_h) = \frac{\ln(1 + 2.34q)}{2.34q} \times \left[\frac{1}{1 + 3.89q + (16.1q)^2 + (5.46q)^3 + (6.71q)^4} \right]^{1/4} \times \left[\left(\frac{1 + 0.01647x^{3.259/2} + 2.803 \times 10^{-5}x^{3.259}}{1 + 10.90x_0^{3.259}} \right)^{\Omega_h^{1.05}} \right]^{1/2}, \quad (2)$$

where $\Gamma = \exp(-2\Omega_b)h$, $q = k/\Gamma h$, $\Gamma_\nu = a^{1/2}\Omega_h h^2$, $x = k/\Gamma_\nu$, $x_0 = x(a=1)$, and k is in unit of Mpc^{-1} . For HDM, it is given by

$$T_h(k, a, \Omega_h) = T_c(k, a, \Omega_h) \times \left[\frac{\exp(-0.0015x')}{1 - 0.121x'^{1/2} + 0.102x' - 0.0162x'^{3/2} + 0.00171x'^2} \right]^{1/2}, \quad (3)$$

where $x' = k/\Gamma_\nu h$. We assume that CDM and baryonic matter have the same power spectrum. Then, the density-weighted power spectrum $P = [\Omega_h P_h^{1/2} + (1 - \Omega_h)P_c^{1/2}]^2$ describes the gravitational perturbations contributed by all the matter components.

The normalization constant A is related to $\sigma_8 \equiv \sigma(R = 8h^{-1}\text{Mpc}, a = 1, \Omega_h)$ by the following relation

$$\sigma^2(R, a, \Omega_h) = \int_0^\infty \frac{dk}{k} 4\pi k^3 P(k, a, \Omega_h) W^2(kR) \quad (4)$$

where $W(kR) = 3[\sin(kR) - kR \cos(kR)]/(kR)^3$ is the top-hat window function. After *COBE*, the rms quadrupole Q_{rms-PS} inferred from the cosmic microwave background anisotropy is often used to fix σ_8 . In the CHDM universe, σ_8 is approximately given by

$$\sigma_8 = Q_{18}(n) \frac{h^2 0.008^{(1-n)/2}}{0.0136 + 0.294h^{0.803} + 0.109h^2} \times \frac{1 + (1 - \Omega_h)^{5.11} 0.116(\Omega_h h)^{-0.893}}{1 + 0.116(\Omega_h h)^{-0.893}}, \quad (5)$$

where $Q_{18}(n) = Q_{rms-PS}(n)/18\mu\text{K}$ (Ma 1996). We take $Q_{rms-PS} = 18\mu\text{K}$ for $n = 1$, $Q_{rms-PS} = 19.2\mu\text{K}$ for $n = 0.9$, and $Q_{rms-PS} = 20.5\mu\text{K}$ for $n = 0.8$, respectively (Górski et al. 1994; Ma 1996).

2.3 Numerical Method

The simulations have been performed with the cosmological hydrodynamic code described in Ryu et al. (1993). It is based on the Total Variation Diminishing (TVD) scheme, which is an explicit, second-order, Eulerian finite difference scheme (Harten 1983). Extra care was taken with the code in two aspects: (1) Strong shocks (with Mach number larger than ~ 100) were identified and handled specially in order to prevent the pre-shock regions from being heated unphysically. (2) Self-gravity and cosmological expansion were included in the way that the total energy conservation represented by the Layzer-Irvine equation (Peebles 1980) is preserved.

Since the core radius of typical X-ray clusters is $\lesssim 0.5h^{-1}\text{Mpc}$ and the cluster-cluster separation is $\sim 50h^{-1}\text{Mpc}$, $\sim 100^3$ is the absolute minimum number of grids required for baryonic matter in order to get statistically meaningful X-ray quantities. The simulations have been done in a periodic computational domain using 256^3 grids, 128^3 CDM particles, and 2×128^3 HDM particles. The initial condition for the HDM particles has been generated in pairs with random and opposite thermal velocities in order to sample neutrino phase space distribution (Klypin et al. 1993). The comoving size of the computational domain is $80h^{-1}\text{Mpc}$, so the grid size is $0.31h^{-1}\text{Mpc}$. While a smaller size would allow us to resolve cluster structure better, a larger size would allow larger waves included and give us a larger sample of high-luminosity and high-temperature clusters. With the domain size of $80h^{-1}\text{Mpc}$, which has been determined by a compromise between the two considerations, clusters are identified comfortably and yet enough clusters are yielded for statistical analyses. However, with the grid size of $0.31h^{-1}\text{Mpc}$, clusters are not “fully” resolved resulting in under-estimate of X-ray luminosities (see §3.2 for further discussion). The simulations have been started at $z = 15$ (or $a = 1/16$) and run to $z = 0$ (or $a = 1$).

In the simulations, atomic processes such as heating and cooling have not been included, as they will have little effect on the hot cluster gas discussed in this paper.

3 RESULTS

3.1 Power Spectrum

We have calculated the linear power spectrum of total (dark and baryonic) matter for the 4 models listed in Table 1 using the formulae in §2.2. Figure 1 shows them as well as the power spectrum reconstructed from galaxy and cluster surveys by Peacock & Dodds (1994). The upper panel contains the power spectra of the models with $h/n/\Omega_h = 0.5/0.9/0.1$ (Model CHDMc and CHDMd) and the lower panel with $h/n/\Omega_h = 0.5/0.9/0.2$ (Model CHDMa and CHDMb). They agree well with the Peacock & Dodds’s reconstructed power spectrum as was already shown by Ma (1996), although the Peacock & Dodds’s power spectrum is for the CDM model. Note that each panel contains a dotted curve for the model with $\Omega_b = 0.05$ and a solid curve for the model with $\Omega_b = 0.1$, although they are not well distinguished. In general, increasing Ω_b with fixed Ω_h results in decreasing power at small scales, but only by a small amount. The plots indicate that the power spectrum is insensitive to the baryonic fraction. The power spectra of other CHDM models with $0.5 \leq h \leq 0.8$, $0.8 \leq n \leq 1$, and $0.05 \leq \Omega_h \leq 0.3$ can be found in Choi (1996).

3.2 Properties of X-ray Clusters

The properties of X-ray clusters are sensitive to Ω_b , since the X-ray bremsstrahlung emission is proportional to the square of gas density. So they can be used to constrain Ω_b . We select two models, Model CHDMa and CHDMb with $h/n/\Omega_h = 0.5/0.9/0.2$ and $\Omega_b = 0.05$ and 0.1 , and study by numerical simulations the properties of X-ray clusters in those models in detail.

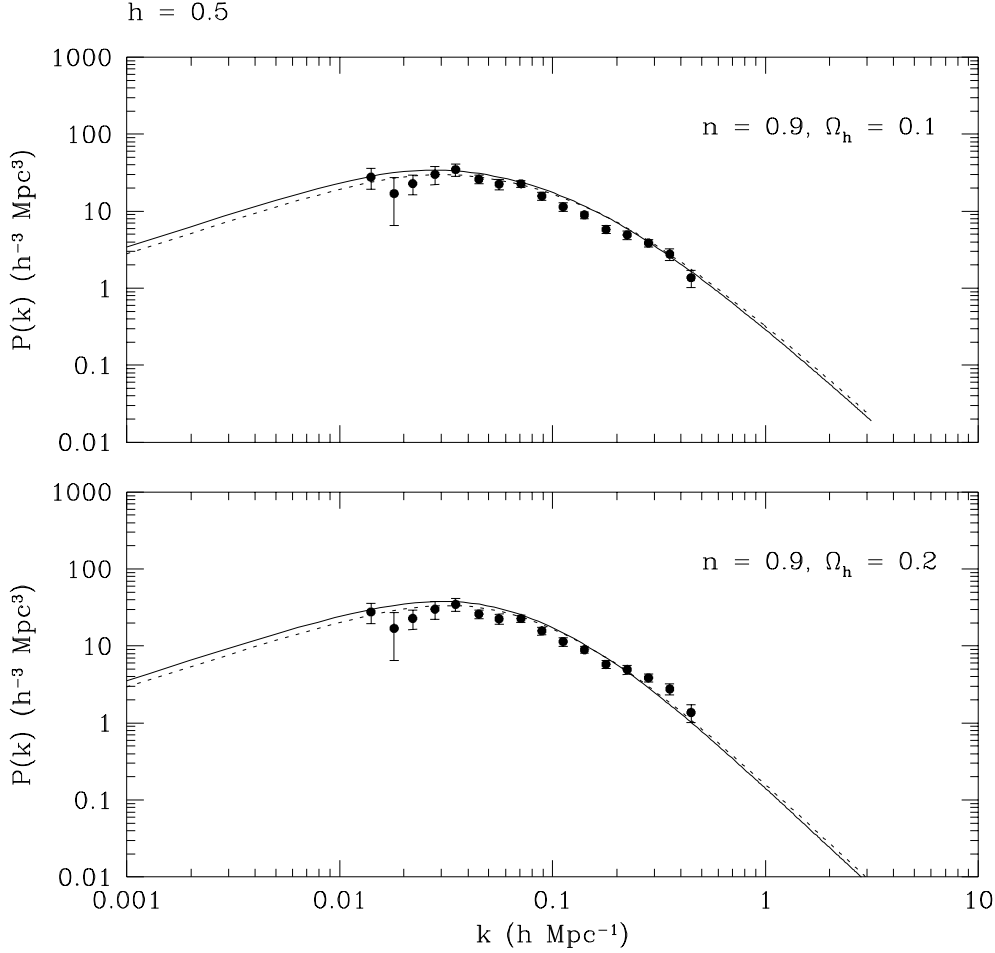


Figure 1. Linear power spectra of total (dark and baryonic) matter for Model CHDMc and CHDMd (upper panel) and CHDMa and CHDMb (lower panel). Each panel contains a dotted curve for the model with $\Omega_b = 0.05$ (Model CHDMc and CHDMa) and a solid curve for the model $\Omega_b = 0.1$ (Model CHDMd and CHDMb). The reconstructed power spectrum from galaxy and cluster surveys is shown with filled circles (Peacock & Dodds 1994).

X-ray clusters emit X-rays from the hot intra-cluster gas that fills the space between galaxies and occupies much of the cluster’s volume. In general the core radius of typical X-ray clusters is about $0.5h^{-1}\text{Mpc}$ and the total radius about $1h^{-1}\text{Mpc}$, but they cannot be accurately determined from observations. The total (bolometric) X-ray luminosity due to the thermal bremsstrahlung is

$$L_x = 4\pi \int_{\nu} \int_V j_{ff} d^3\mathbf{r} d\nu \quad (6)$$

where j_{ff} is given in units of $\text{erg cm}^{-3}\text{s}^{-1}\text{Hz}^{-1}\text{sr}^{-1}$ by

$$j_{ff} = \frac{1}{4\pi} \frac{32e^4}{3m_e^2c^3} \left[\frac{\pi h\nu_0(\text{H})}{3kT} \right]^{1/2} \exp\left(-\frac{h\nu}{kT}\right) \times g_{ff}(T, \nu) [n(\text{HIII}) + n(\text{HeII}) + 4n(\text{HeIII})] n(e). \quad (7)$$

$g_{ff}(T, \nu)$ is the Gaunt factor. We assume the primordial abundance, 76% H and 24% He by mass, and that H and He are fully ionized.

X-ray clusters in the simulations are identified as follows. We first calculate the total X-ray luminosity due to the thermal bremsstrahlung in each cell. The cells with the total X-ray luminosity higher than 10^{38}erg s^{-1} are selected

as X-ray bright cells. Then, we find the local maxima by comparing the total X-ray luminosity of each X-ray bright cell with that of 124 neighboring cells, and identify them as the centers of the X-ray clusters. Having identified the X-ray cluster centers, we define the X-ray clusters in the whole computational domain. The total X-ray cluster volume consists of 125 cells, the central cell and 124 cells surrounding it. For the calculations of X-ray luminosity and temperature, each cell is weighted equally by a weight factor $= 4\pi/3 (\text{radius})^3/(\text{resolution})^3/(\text{the number of cells}) = 4\pi/3 (1.0)^3/(0.31)^3/125 = 1.098$, so that the total volume of each X-ray cluster equals the volume of a sphere of radius $1h^{-1}\text{Mpc}$. The weighting scheme compensates for the adoption of a slightly small volume by heightening the weight per cell.

We note that our scheme is similar to (but not same as) that used by Kang et al. (1994), Cen & Ostriker (1994), and Bryan et al. (1994a), but different from that used by Bryan et al. (1994b). Our test showed that the calculated luminosity and temperature are insensitive to the details of the scheme, as already pointed by Bryan et al. (1994b). However, as pointed in those previous works, our luminosity should have been under-estimated due to insufficient reso-

Figure 2. Projected distribution of the X-ray clusters with $L_x > 10^{41} \text{erg s}^{-1}$ from the region of $r \leq 1h^{-1} \text{Mpc}$. The open circles in the left panels represent the X-ray clusters in CHDMa, and the filled circles in the right panels represent the X-ray clusters in CHDMb.

lution to resolve the central density structure in clusters. Bryan et al. (1994b) pointed that in their simulation with resolution similar to ours, the under-estimation in the luminosity could be as high as a factor of 3. The importance of resolution was also pointed by Evrard, Metzler & Navarro (1996) in the study of X-ray clusters using the SPH code. On the other hand, the calculated temperature is relatively insensitive to resolution.

The bright X-ray clusters with $L_x > 10^{41} \text{erg s}^{-1}$ from the region of radius $1h^{-1} \text{Mpc}$ at $z = 0$ are shown in Figure 2. Left panels show the projection of the X-ray clusters generated in CHDMa in the $x-y$, $y-z$, and $z-x$ planes, and the right panels show the projection of the X-ray clusters generated in CHDMb. The distribution pattern of the X-ray clusters is similar, but there are more X-ray clusters in CHDMb (with larger Ω_b) than in CHDMa. In CHDMa, our computational domain with $(80h^{-1} \text{Mpc})^3$ volume at $z = 0$ contains no cluster with total luminosity brighter than $10^{45} \text{erg s}^{-1}$, no cluster brighter than $10^{44} \text{erg s}^{-1}$, 13 clusters brighter than $10^{43} \text{erg s}^{-1}$, 44 clusters brighter than $10^{42} \text{erg s}^{-1}$, and 268 clusters brighter than $10^{41} \text{erg s}^{-1}$. In CHDMb, our computational domain at $z = 0$ contains no cluster with total luminosity brighter than $10^{45} \text{erg s}^{-1}$, 2 clusters brighter than $10^{44} \text{erg s}^{-1}$, 24 clusters brighter than $10^{43} \text{erg s}^{-1}$, 126 clusters brighter than $10^{42} \text{erg s}^{-1}$, and 558 clusters brighter than $10^{41} \text{erg s}^{-1}$.

The luminosity functions calculated with the identified X-ray clusters are shown in Figures 3a and 3b for CHDMa and CHDMb. The plots show the luminosity functions in $10^{40} \text{erg s}^{-1} \leq L_x \leq 10^{45} \text{erg s}^{-1}$ and $0 \leq z \leq 1$. There are very few high-luminosity clusters with $L_x \gtrsim 10^{44} \text{erg s}^{-1}$, because our computational domain is too small to contain them. Also the plots show the observed bolometric luminosity function $\{3.1_{-1.8}^{+4.5} \times 10^{-6} h^3 \text{Mpc}^{-3} h^2 [L_{44}(\text{bol})]^{-1}\} [h^2 L_{44}(\text{bol})]^{-1.85 \pm 0.4}$ by Henry & Arnaud (1991) as the boxed area. The Henry & Arnaud's luminosity function agrees with the more recently considered ones, such as the one by Burn et al. (1996), although White, Efstathiou & Frenk (1993) pointed errors in the Henry & Arnaud's luminosity function. The observed bolometric luminosity function is more consistent with the calculated luminosity function of CHDMa than that of CHDMb. A possible correction for the under-estimation of the X-ray luminosity would make the discrepancy between the calculated luminosity function of CHDMb and the observed luminosity function worse.

Also in CHDMb we find weak positive evolution until $z \sim 0.2$, and then mild negative evolution thereafter. This can be seen in Figure 4 which shows the number density evolution of X-ray clusters with $L_x > 10^{43} \text{erg s}^{-1}$ between $z = 0$ and $z = 1.5$. Open circles are for CHDMa and filled circles are for CHDMb. We note that the evolution of the cluster abundance does not agree with the analytic predictions such as the one based on the Press-Schechter approximation (Bahcall, Fan & Cen 1997; Fan, Bahcall, & Cen 1997), according to which the evolution is much steeper in high Ω and low σ_8 models.

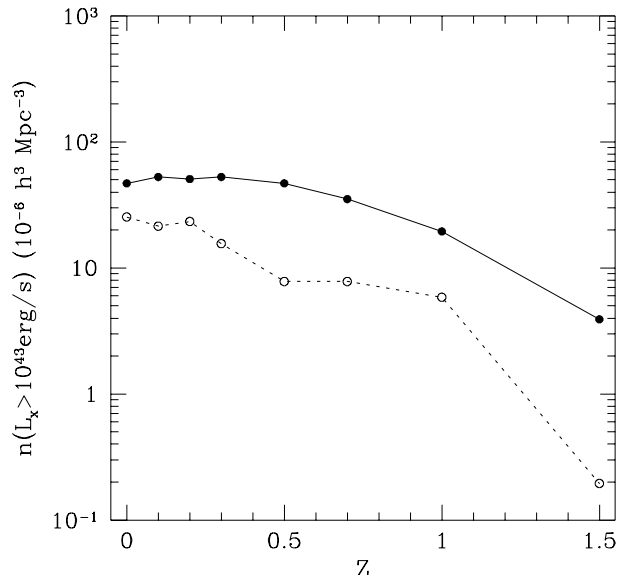


Figure 4. Evolution of the number density of the X-ray clusters with $L_x > 10^{43} \text{erg s}^{-1}$ from the region of $r \leq 1h^{-1} \text{Mpc}$. The open circles and dotted line are for CHDMa, and the filled circles and solid line are for CHDMb.

We fit the luminosity function to an approximate Schechter function

$$n(L)dL \equiv n_0 \left(\frac{L}{L^*}\right)^{-\alpha} \exp\left(-\frac{L}{L^*}\right) \frac{dL}{L^*} \quad (8)$$

using the Levenberg-Marquardt method, and determine the Schechter parameters (α , L^* , n_0) as a function of redshift. The parameters are calculated at seven different redshifts and listed in Table 2. Here, L^* is in unit of $10^{44} \text{erg s}^{-1}$ and n_0 is in unit of $10^{-6} h^3 \text{Mpc}^{-3}$. The Schechter functions with these parameters are plotted with dotted lines for CHDMa and solid lines for CHDMb in Figure 3. The value of the Schechter α -parameter in CHDMa, ~ 1.7 , is slightly larger than that in CHDMb, but still smaller than the best-fit observational values, $1.9 - 2.0$ quoted by Henry (1992). However, the Schechter α -parameters in our simulations are primarily determined by lower luminosity clusters than those used for the fits of observational data (Henry 1992). The characteristic luminosity, L^* , and the total number density, n_0 , of the Schechter luminosity function are determined less reliably, because the number of samples is too small.

The temperature distribution function, in addition to the luminosity function, of X-ray clusters provides a useful test for the structure formation theory. It has been calculated at four different redshifts and shown in Figures 5a and 5b for CHDMa and CHDMb. The turnover at low X-ray temperature, T_x , is possibly caused by our definition of minimum cell luminosity to constitute X-ray bright cells. There are almost no high-temperature clusters with $T_x \gtrsim 10 \text{keV}$. Again, this is due to the limited volume of our computational domain which is not big enough to contain high-temperature clusters. The observed temperature distribution function is $(1.8_{-1.5}^{+0.8} \times 10^{-3} h^3 \text{Mpc}^{-3} \text{keV}^{-1})(kT)^{-4.7 \pm 0.5}$ according to

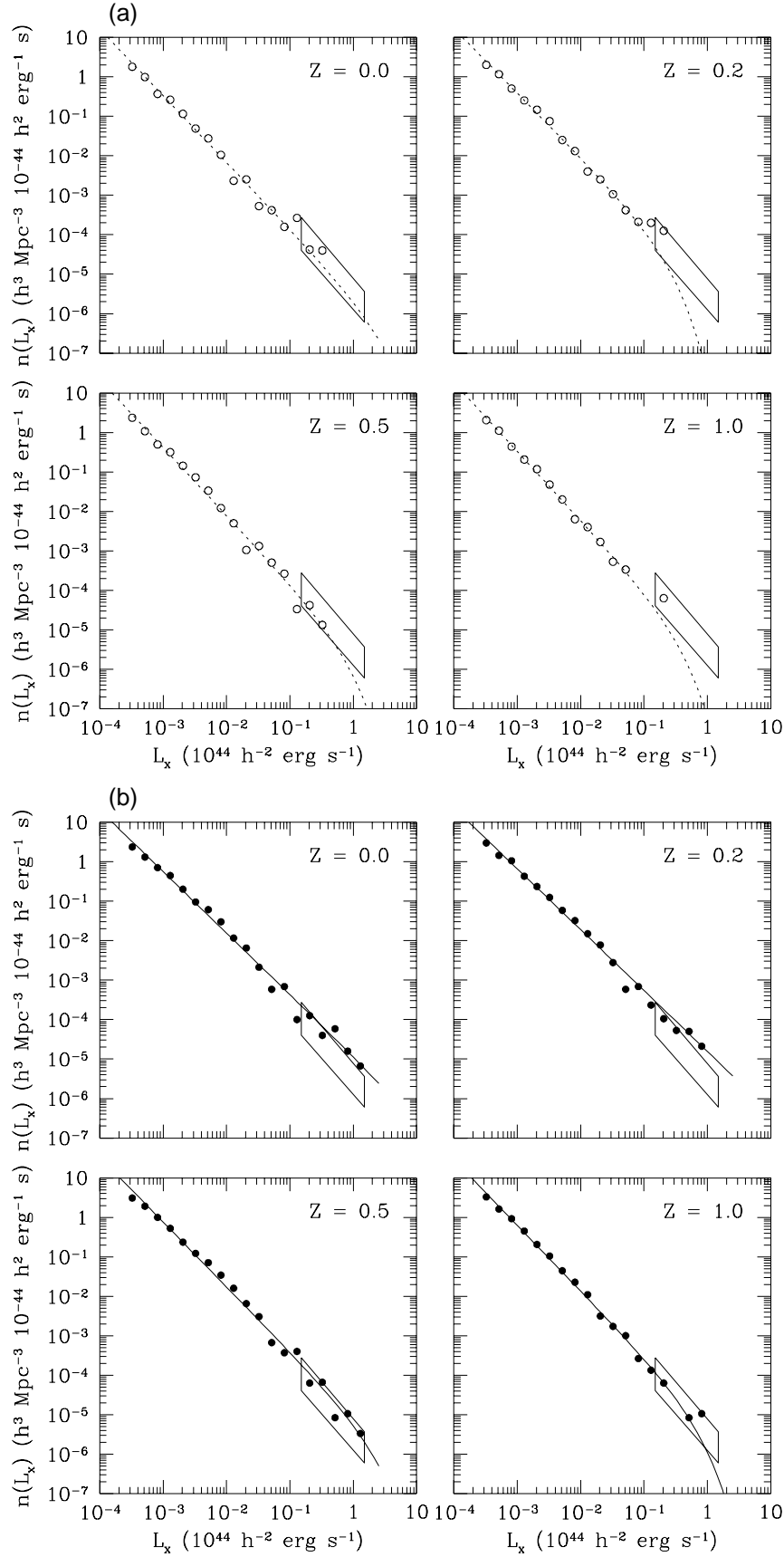


Figure 3. Luminosity function of the X-ray clusters at four different epochs with X-ray luminosity from the region of $r \leq 1h^{-1}\text{Mpc}$ integrated over the whole frequency range. The open circles in (a) represent the luminosity function in CHDMA, and the filled circles in (b) represent the luminosity function in CHDMb. The dotted and solid lines are the Schechter fits, and the boxed area shows the observational data (Henry & Arnaud 1991).

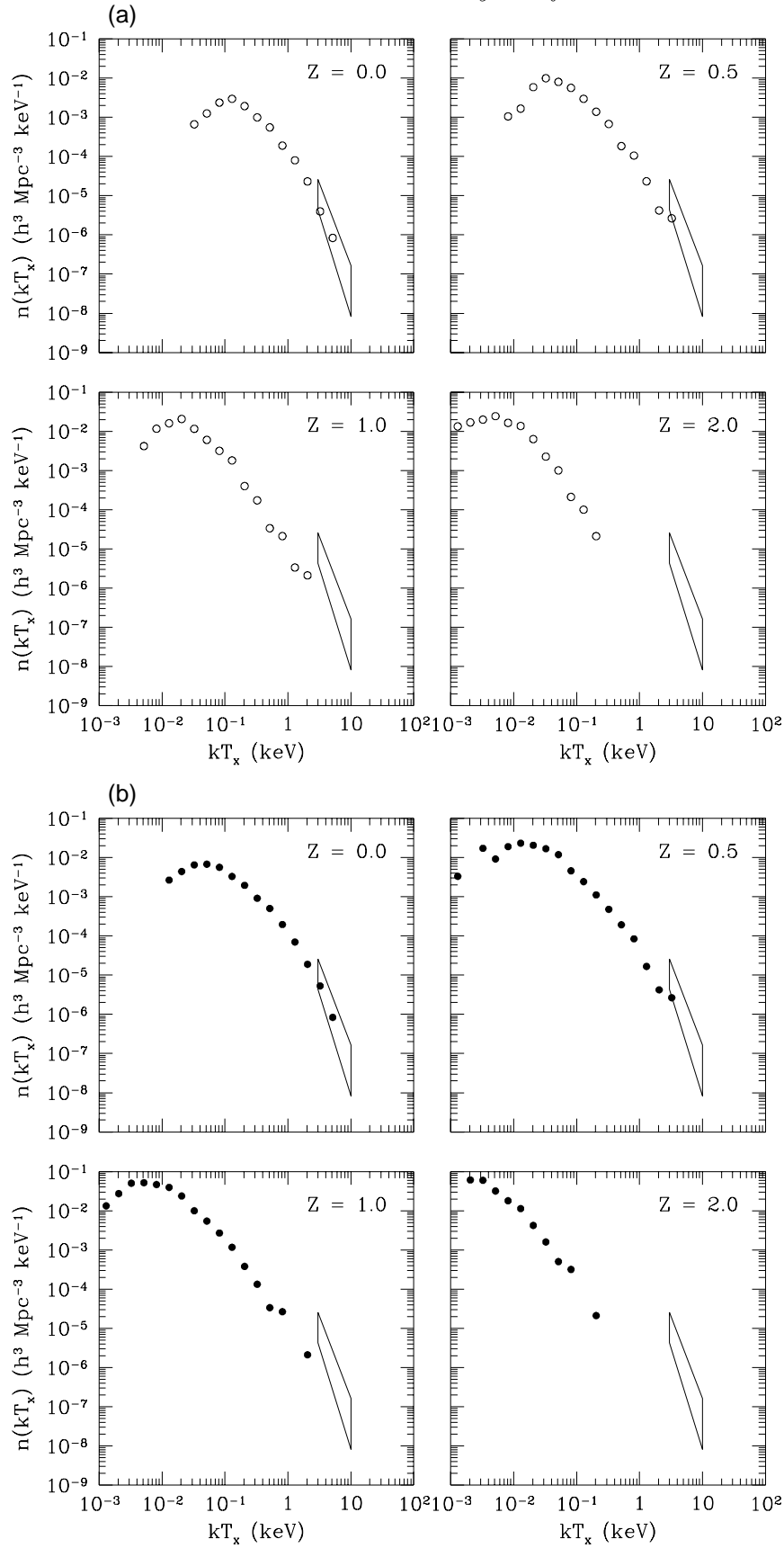


Figure 5. Temperature distribution function of the X-ray clusters at four different epochs. The open circles in (a) represent the distribution function in CHDMa, and the filled circles in (b) represent the distribution function in CHDMb. The boxed area shows the observation data (Henry & Arnaud 1991).

Table 2. Schechter fits for the X-ray clusters luminosity function.

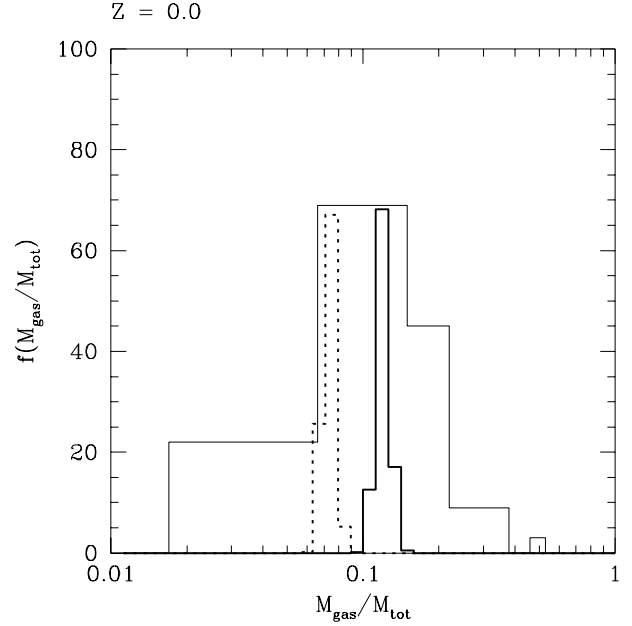
Model	z	α	L^*	n_0
CHDMa	0.0	1.69	2.51	1.48
	0.1	1.55	0.04	47.27
	0.2	1.64	0.19	13.76
	0.3	1.61	0.30	11.57
	0.5	1.72	0.67	3.85
	0.7	1.71	0.31	6.64
1.0	1.74	0.29	4.95	
CHDMb	0.0	1.56	14.48	2.69
	0.1	1.56	23.22	2.37
	0.2	1.54	86.69	1.41
	0.3	1.57	1.09	12.96
	0.5	1.65	1.87	5.89
	0.7	1.67	2.03	4.60
1.0	1.67	0.57	9.31	

Figure 6. Relation of T_x versus L_x at $z = 0$. The open circles in the upper panel are from CHDMa, and the filled circles in the lower panel is from CHDMb. The dotted and solid lines show the best fits, and the boxed area indicates the observational data (Henry & Arnaud 1991).

Henry & Arnaud (1991), and shown as the boxed area. In the reliable range of T_x , the distribution functions for the both models are almost identical. This is expected, since T_x is mainly determined by the gravitational potential of *total* matter. Both the distribution functions agree well with the observed data.

The relation between the cluster's temperature, T_x , and luminosity, L_x , should be less sensitive to the normalization of power spectrum. In Figure 6, we show the plots of T_x versus L_x at $z = 0$. The upper panel is for CHDMa and the lower panel is for CHDMb. The boxed area indicates the observed relation, $\log_{10} T_x (\text{keV}) = \log_{10} (4.2_{-0.8}^{+1.0}) + (0.265 \pm 0.035) \log_{10} (h^2 L_{44})$ according to Henry & Arnaud (1991). The best straight-line fits, $\log_{10} kT_x = A + B \log_{10} L_x$, are shown as a dotted line for CHDMa and solid line for CHDMb. $A = 0.672$ and $B = 0.413$ for CHDMa, and $A = 0.495$ and $B = 0.466$ for CHDMb, respectively. For a given luminosity, the temperature is somewhat lower for CHDMb ($A = 0.495$) than for CHDMa ($A = 0.672$), and the slopes ($B = 0.413$ and 0.466) are somewhat steeper than that indicated by observations ($B = 0.265 \pm 0.035$). However, the observed slope is determined mainly by high-luminosity clusters. We find that in the region where comparison can be made, the agreement with the observations is better for CHDMa than CHDMb.

For each simulated X-ray cluster, the gas mass and the total mass within a sphere of radius $1h^{-1}\text{Mpc}$ are calculated at $z = 0$. The histogram of the ratio of the two masses is shown in Figure 7. The thick dotted histogram shows the ratio distribution for CHDMa, and the thick solid shows the ratio distribution for CHDMb. These histograms are arbitrarily normalized to have a peak height similar to the observation data, which is drawn with the thin solid histogram, adopted from Jones & Forman (1992). The more recent observed ratio of the gas to total mass is $(M_{gas}/M_{tot})_{obs} = 0.1 - 0.22$ for a refined sample of 13 clusters (White & Fabian 1995), so the observed ra-

**Figure 7.** Histogram of the ratio of gas to total mass in the X-ray clusters with $L_x > 10^{41} \text{erg s}^{-1}$ at $z = 0$. The thick dotted line represents the histogram from CHDMa, and the thick solid shows the histogram from CHDMb. The thin solid line shows the observational data (Jones & Forman 1992).

tio has gone up a little. The median of the computed ratio is $(M_{gas}/M_{tot})_{com} = 0.0731 \pm 0.0038$ for CHDMa and $(M_{gas}/M_{tot})_{com} = 0.120 \pm 0.0069$ for CHDMb. Improving observations will probably narrow the observed histogram, while increasing the dynamical range of numerical simulations and incorporating more realistic physics will widen the computed histograms. Both expected improvements should make the agreement better.

Figure 8 shows the evolution of the average X-ray temperatures for clusters with $L_x > 10^{43} \text{erg s}^{-1}$ from $z = 0$ to $z = 1.5$. Open circles are for CHDMa and filled circles are for CHDMb. Also shown are the best-fits to the evolution analytically predicted by Kaiser (1986), $T_x \propto (1+z)^{-1}$ for $\Omega = 1$. The evolutions for the both model are similar, as expected. But there is an overall difference that the average temperatures are smaller in CHDMb by a factor of 0.65 than those in CHDMa. The computed evolution of the average temperatures agrees only marginally with analytical prediction by Kaiser (1986).

4 CONCLUSION

We have computed the linear power spectrum of total matter for spatially flat, *COBE*-normalized CHDM models. We have found that the models with $h/n/\Omega_h = 0.5/0.9/0.1$ and $0.5/0.9/0.2$ give a power spectrum in good agreement with the observed power spectrum. Then, through numerical simulations that include the hydrodynamics of baryonic matter, as well as the particle dynamics of dark matter, we have computed the properties of X-ray clusters for the models with $h/n/\Omega_h = 0.5/0.9/0.2$ and $\Omega_b = 0.05$ and 0.1 . We have found that the models with $\Omega_b = 0.05$ produce X-ray clusters with properties that agree well with the observed data.

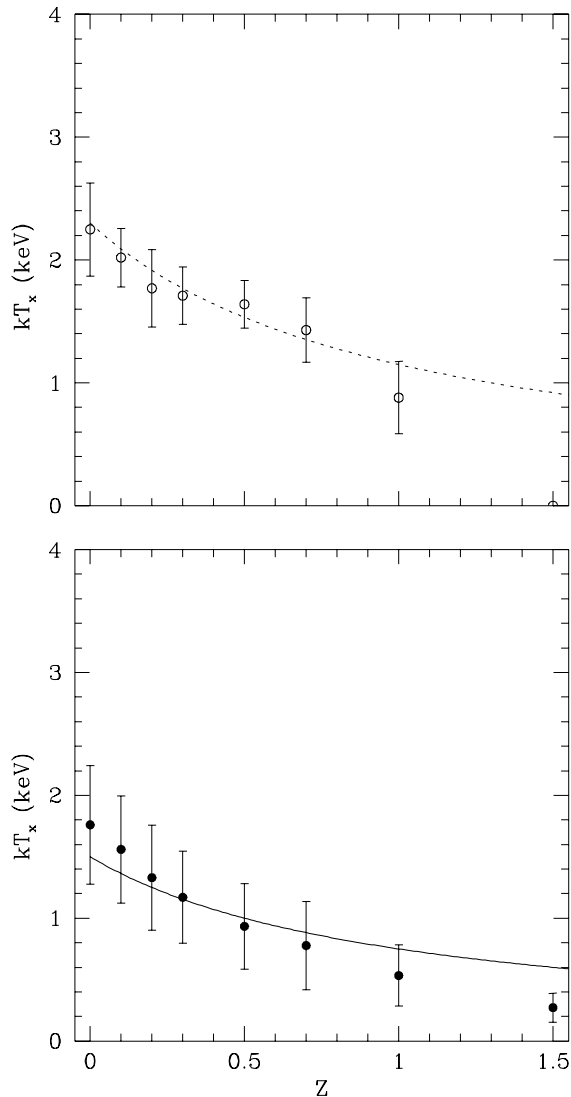


Figure 8. Average X-ray temperature for the clusters with $L_x > 10^{43} \text{ erg s}^{-1}$ as a function of redshift. The open circles in the upper panel is from CHDMa, and the filled circles in the lower is from CHDMb. The dotted and solid curves show the best-fits to the evolution predicted by Kaiser (1986), $T_x \propto (1+z)^{-1}$.

Our results have shown that the physical properties of X-ray clusters considered in this paper are quite sensitive to Ω_b , since the bremsstrahlung emission is proportional to ρ_b^2 . Although the number of X-ray bright clusters in the model with $\Omega_b = 0.1$ exceeds slightly the observed number, we still consider the model to be marginally consistent with observations. However, the *COBE*-normalized CHDM model with $\Omega_b > 0.1$ may be ruled out by the present work. Finally, we note that that our simulations are not fully converged, so X-ray luminosity may have been under-estimated by a factor of 3 or more. Hence, future simulations with higher resolution will put a more stringent constraint on Ω_b .

ACKNOWLEDGMENTS

This work is based on the Master's thesis of EC at Kyungpook National University in Korea. The simulations were

performed on Cray-C90 at Systems Engineering Research Institute in Korea. We are grateful to Drs. H. Kang and J. Hwang for discussions, and the referee, Dr. J. Primack, for suggestions and comments on the manuscript. The work by EC was supported in part by KOSEF grant No. 961-0203-013-1. The work by DR was supported in part by Seoam Scholarship Foundation and by KOSEF through the 1997 Korea-US Cooperative Science Program.

REFERENCES

- Achilli S., Occhionero F., Scaramella R., 1985, *ApJ*, 299, 577
 Bahcall, N. A., Fang, X., Cen, R., 1997, *ApJ*, in press
 Bi H., Ge J., Fang L.-Z., 1995, *ApJ*, 452, 90
 Bonometto S. A., Borgani S., Ghigna S., Klypin A., Primack J. R., 1995, *MNRAS*, 273, 101
 Borgani S., Plionis M., Coles P., Moscardini L., 1995, *MNRAS*, 277, 1191
 Borgani S. et al., 1997, *New Astronomy*, 1, 321
 Bryan G. L., Cen R., Norman M. L., Ostriker J. P., Stone J. M., 1994a, *ApJ*, 428, 405
 Bryan G. L., Klypin A., Loken C., Norman M. L., Burns J. O., 1994b, *ApJ*, 437, L5
 Bunn E. F., Scott D., White M., 1995, *ApJ*, 441, L9
 Burn, J. O., Ledlow, M. J., Loken, C., Klypin, A., Voges, W., Bryan, G. L., Norman, M. L., White, R. A., 1996, *ApJ*, L49.
 Cen R., Ostriker J. P., 1994, *ApJ*, 429, 4
 Choi E., 1996, Master's thesis, Kyungpook National University
 Copi C., Schramm D., Turner M., 1995, *Science*, 267, 192
 Davé R., Hellinger D., Primack J., Nolthenius R., Klypin A., 1997, *MNRAS*, in press
 Davis M., Summers F. J., Schlegel D., 1992, *Nature*, 359, 393
 Dodelson S., Gates E., Stebbins A., 1996, *ApJ*, 467, 10
 Evrard, A. E., Metzler, C. A., Navarro, J. F., 1996, *ApJ*, 469, 494
 Fang L. Z., Li S. X., Xiang S. P., 1984, *A&A*, 140, 77
 Fang, X., Bahcall, N. A., Cen, R., 1997, preprint (astro-ph/9709265)
 Ghigna S., Borgani S., Bonometto S. A., Guzzo L., Klypin A., Primack J. R., Giovanelli R., Haynes M., 1994, *ApJ*, 437, L71
 Górski K. M., Hinshaw G., Banday A. J., Bennett C. L., Wright E. L., Kogut A., Smoot G. F., Lubin P., 1994, *ApJ*, 430, L89
 Harten A., 1983, *J. Comp. Phys.*, 49, 357
 Henry J. P., 1992, in Fabian A. C., ed, *Clusters and Superclusters of Galaxies*. Kluwer, Dordrecht, p.311
 Henry J. P., Arnaud K. A., 1991, *ApJ*, 372, 410
 Holtzman J. A., Primack J. R., 1993, *ApJ*, 405, 428
 Jing Y.-P., Fang L.-Z., 1994, *ApJ*, 432, 438
 Jing Y. P., Mo H. J., Börner G., Fang L. Z., 1994, *A&A*, 284, 703
 Jones C., Forman W., 1992, in Fabian A. C., ed, *Clusters and Superclusters of Galaxies*. Kluwer, Dordrecht, p.49
 Kaiser N., 1986, *MNRAS*, 222, 323
 Kang H., Cen R., Ostriker J. P., Ryu D., 1994, *ApJ*, 428, 1
 Kauffmann G., Charlot S., 1994, *ApJ*, 430, L97
 Kitayama T., Suto Y., 1996, *ApJ*, 469, 480
 Klypin A., Rhee G., 1994, *ApJ*, 428, 399
 Klypin A., Holtzman J., Primack J., Regös E., 1993, *ApJ*, 461, 1
 Klypin A., Borgani S., Holtzman J., Primack J., 1995, *ApJ*, 444, 1
 Klypin A., Nolthenius R., Primack J., 1997, *ApJ*, 474, 533
 Lubin L. M., Cen R., Bahcall N. A., Ostriker J. P., 1995, *ApJ*, 460, 10
 Ma C.-P., 1996, *ApJ*, 471, 13
 Ma C.-P., Bertschinger E., 1994, *ApJ*, 434, L5
 Mo H. J., Miralda-Escudé J., 1994, *ApJ*, 430, L25
 Nolthenius R., Klypin A., Primack J., 1994, *ApJ*, 422, L42
 Ostriker J. P., Steinhardt P. J., 1995, *Nature*, 377, 600

- Peacock J. A., Dodds S. J., 1994, MNRAS, 267, 1020
Peebles P. J. E., 1980, *The Large-Scale Structure of the Universe*.
Princeton Univ. Press, Princeton
Pogosyan D. Y., Starobinsky A. A., 1995, ApJ, 447, 465
Primack J. R., Holtzman J., Klypin A., Caldwell D. O., 1995,
Phys. Rev. Lett., 74, 2160
Ryu D., Ostriker J. P., Kang H., Cen R., 1993, ApJ, 414, 1
Schaefer R. K., Shafi Q., Stecker F. W., 1989, ApJ, 347, 575
Valdarnini R., Bonometto S. A., 1985, A&A, 146, 235
Van Dalen A., Schaefer R. K., 1992, ApJ, 398, 33
Walter C., Klypin A., 1996, ApJ, 462, 13
Walker T. P., Steigman G., Schramm D. N., Olive K. A., Kang
H. S., 1991, ApJ, 376, 51
White D. A., Fabian A. C., 1995, MNRAS, 273, 72
White, S. D. M., Efstathiou, G., Frenk, C. S., 1993, MNRAS, 262,
1023.
Yepes G., Klypin A., Campos A., Fong R., 1994, ApJ, 432, L11

This paper has been produced using the Royal Astronomical
Society/Blackwell Science L^AT_EX style file.

This figure "fig2.gif" is available in "gif" format from:

<http://arxiv.org/ps/astro-ph/9710078v1>

This figure "fig6.gif" is available in "gif" format from:

<http://arxiv.org/ps/astro-ph/9710078v1>